Experimental Mechanics
DOI 10.1007/s11340-009-9313-y

Measurement of Strain/Load Transfer in Parallel Seven-wire Strands with Neutron Diffraction

I.C. Noyan · A. Brügger · R. Betti · B. Clausen

Received: 8 July 2009 / Accepted: 3 November 2009

Abstract The elastic strains induced in the constituent wires of parallel wire strands under tensile loading were measured using neutron diffraction. The elastic strains carried by the individual wires depended very strongly on the boundary conditions at the grips and on radial clamping forces. The friction forces between the wires were quite significant and should not be neglected in analytical or numerical formulations of strain partitioning in parallel wire cables.

Keywords Neutron strain measurement · Bridge cable · Parallel cable · Load sharing

Introduction

Main cables of suspension bridges are the most critical elements in these structures. Such cables are made of many thousands of parallel high-strength steel wires, whose diameter is about 5 mm. The core of the cable consists of closely-packed galvanized steel wire bundles (strands) (Fig. 1). Each bundle consists of many parallel steel wires whose number depends on the type of cable spinning process used. Inner strands usually have hexagonal cross-sections to optimize the compaction operation. For prefabricated Parallel Wire Strands (PWS), each hexagonal strand is composed of 127 wires. The cross-sections of the strands adjoining the periphery are adjusted so as to give the entire cable core a circular cross-section after compaction. The core is wrapped by a continuous, pre-tensioned wire layer, and it is radially clamped at regular intervals along its entire length to ensure geometrical integrity and tightness, and to enhance strain transfer to any broken wires. Some of the clamping action is also provided by the cable bands that serve as attachment points for the vertical suspenders that connect the bridge deck to the main cable. A mid-sized bridge cable, such as the one used in the Manhattan Bridge in New York, can be about 50 cm (20”) in diameter, with about 8,500–9,000 wires while larger cables, approximately 0.9 m to 1 m in diameter (e.g. the Golden Gate Bridge, Verrazano Narrows Bridge and the George Washington Bridge), contain about 26,000–28,000 wires. Suspension-bridge cables are loaded in tension: they transfer the entire weight of the bridge deck and any traffic that might be on it, more than several hundred thousand tons, to the suspension towers, and to anchor points at each end of the bridge.

Analysis of load partitioning within such cables is a non-trivial problem [1, 2] and poses theoretical [3] and experimental challenges [4–6]. The cable can be considered as a massive fiber composite structure that is loaded in the far field. At a location remote from the ends the local stress state within any wire depends on the far-field stress and the local boundary conditions. These local stress/strain states within the cable at the wire level are very hard to calculate since the boundary conditions such as the friction coefficient at the points of contact, local wire flattening, and local

I.C. Noyan (✉)
Department of Applied Physics and Applied Mathematics,
Columbia University,
New York, NY, USA
e-mail: icn2@columbia.edu

A. Brügger · R. Betti
Department of Civil Engineering and Engineering Mechanics,
Columbia University,
New York, NY, USA

B. Clausen
LANSCE-LC, Los Alamos National Laboratory,
Los Alamos, NM, USA

Published online: 12 December 2009

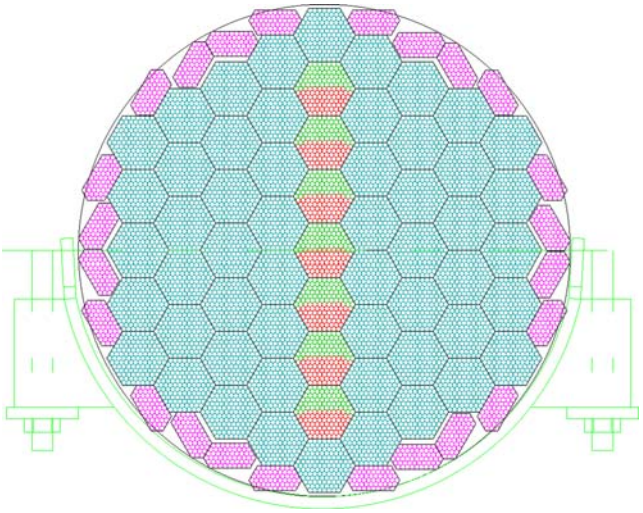

Fig. 1 Hexagonal wire bundles of a bridge cable. The inner bundles are closely-packed hexagonal structures. The shapes of the outer bundles are adjusted to give a circular perimeter. The outline of a cable clamp is also shown

contact areas cannot be easily measured or estimated. In addition, because of deterioration or local manufacturing defects, there may be broken wires within the cable, which modify the local stress state in such wires. In such cases, local shear forces set-up between the fractured wire and its unbroken neighbors can transfer the axial load to the broken wire so that the broken wire can regain its share of the load away from the fracture point. The development length, L_D, also termed the "recovery length" defines the distance over which a broken wire takes up its full share of the axial load, measured from the fractured end.[1] L_D depends on the local radial forces, contact areas and the coefficients of friction between the broken wire and its immediate neighbors. There are numerical models which can be used to calculate this transfer length [7], but we were not able to locate any experimental measurements of L_D.

In this study we used neutron diffraction to measure the partitioning of applied tensile load between the individual wires of two standard seven-wire test strands. In the first case, (A), all of the wires were continuous between the sockets that transmitted the applied tensile load. In the case of ideal grips, where the load is partitioned equally between all of the wires within the strand, such a sample is expected to have the same elastic strain within all strands. In the second case, (B), the center wire of the strand was free from the grips and load could only be transmitted to this wire through shear, or through mechanical interference within the strand; we used cable clamps to control the efficiency of strain transfer to the center wire. Our results indicate that the standard conical grips are not ideal; upon tensile loading the individual wires of sample A sustained significantly different elastic strains. Results from Sample B showed that friction between the individual wires is an important mode of strain transfer. Even in the fully unclamped case we observed 40% load transfer to the center wire at mid-point of Sample B, indicating that our sample length (310 mm) was comparable to the recovery length in this test geometry. Our results indicate that neutron diffraction can be a very valuable tool in bridge cable and wire rope evaluation.

Experimental

Sample Preparation

Two standard seven-wire test strands [5, 8] were constructed using 5 mm diameter (0.192") galvanized (A coat) ASTM A586 steel wire[2] (Table 1). The outer (six) wires of the strands were centered at the vertices of a regular hexagon [Fig. 2(a)]. The seventh wire was located at the center. The strand ends were inserted into conical socket assemblies [9] machined from commercially available universal joints (Curtis CJ653).[3] The individual wires were then broomed (splayed) out [Fig. 2(b)], and the sockets filled with a commercially available socket epoxy.[4] The socket cavities were truncated cones 40 mm high, with base and top diameters of 40 mm and 15 mm respectively. In the case of sample (A), all of the wires, perimeter and center, were fed into the grips and broomed out. In the case of sample B, only the six perimeter wires were captured in the socket assembly; the central wire terminated approximately 10 mm before the socket assemblies at each end. To ensure proper constraint, a short section of wire was inserted into each socket to take up the volume vacated by the central wire. The outer wires of Sample B at each end were arc-welded to this central stub using flux-core welding wire before they were broomed out. The purpose of the welding was to keep the central stub centered and ensure that all of the wires had equal boundary conditions. The brooming-out operation fractured some of the welds. However, there was enough constraint to keep the central stubs centered while the cavities were filled with epoxy.

[1] This length is analogous to the critical length in shear-lag formulations.

[2] The wires were taken from a standard 152.4 cm diameter (60") reel and exhibited significant curvature. They were used without straightening.

[3] Curtis Universal Joint Company, http://www.curtisuniversal.com/index.html

[4] Socktfast Resin Compound by ESCO® (http://www.escocorp.com/markets/rigging/socketfast.html)

Table 1 Composition and selected bulk mechanical properties of the ASTM A586 hot-rolled wire used in constructing the seven-wire strands. The values shown are averages from seven measurements reported by the supplier. The values in parentheses are the standard deviations. For this alloy, the Young's modulus and Poisson's ratio are approximately 210 GPa and 0.3 respectively [20]

Chemical composition (%)						Mechanical properties		
C	Mn	P	S	Si	Fe	0.7% Stress (MPa)	UTS (MPa)	Elongation (%)
0.84	0.77	0.009	0.005	0.22	Balance	1231 (35)	1765 (8)	6.2 (0.9)
			Minimum ASTM A586 values ➔			1103	1517	4.00

In-situ Loading

The samples were loaded in tension, under load control, on a custom-built horizontal 250 kN hydraulic load frame which is built into the SMARTS neutron diffractometer [10]. During the experiments the total applied load and cross-head displacement were recorded. In addition, the macroscopic strain in one of the bottom wires of the bundle was monitored through an attached extensometer and recorded. The grips and extensometer placement are shown in Fig. 3; the sample shown is strand B, identifiable through the two clamps[5] near each end. This sample was tested in "*tightly-clamped*", "*loosely-clamped*" and "*unclamped*" conditions. In the tightly-clamped case, the nuts of the wire clips at each end of the sample had been tightened to 135 N-m. In the loosely clamped case, these nuts were completely loosened, tightened to 14 N-m, and then loosened, and then tightened again to finger tight. In the third case, one clamp was completely removed, and the other one was moved close to the center of the bundle, and clamped finger-tight; this served to keep the wires in position. Sample A had no clamps, and was tested through a single load cycle. Before the neutron measurements both samples, A and B, were pre-stressed by loading to 350 MPa and then unloading to 50 MPa three times to minimize any relaxation and/or rearrangement that might occur in the grips. After this preloading, we proceeded to the neutron measurement, where the nominal applied loads were kept below 300 MPa.

Neutron Diffraction Measurements

A schematic of the SMARTS instrument is shown in Fig. 4. There are two detector banks, each consisting of 196 ^{3}He filled tubes, which are located 1.5 m from the sample, and are oriented ±90° with respect to the incident neutron beam. The detectors subtend approximately 30° in the horizontal and vertical planes. The sample, mounted in the horizontal load frame, is usually oriented at 45° to the incident neutron beam.[6] The probe volume, i.e., the sample volume scattering into the detectors (Fig. 4, inset), is defined by the incident beam slits ("S" in Fig. 3) and diffracted-beam radial collimators ("RC" in Fig. 3) placed in front of each detector bank [12]. These limit the angular span of the detectors in the horizontal plane to approximately 20°. In the current study, the dimensions of the incident beam cross-section were 2 mm×2 mm, and the radial collimators in front of both detector banks had 2 mm acceptance lengths, resulting in a cuboidal gauge volume of approximately $2\times2\times2$ mm^3. Once set, this probe volume is invariant; during strain mapping the sample is translated to bring different regions of interest in coincidence with the probe volume. In SMARTS, the entire load-frame is mounted on a precision table that permits independent translations, with 10 μm resolution, along two orthogonal axes, *x, y*, in the plane of loading, and along a third axis, *z*, normal to this plane. As shown in Fig. 4, we define the axis along the length of the wire bundle as "*y*", the axis normal to strand cross-section as "*x*", and the axis normal to the load-frame table as "z"; the position $x=0$, $y=0$, $z=0$ denotes the center point of the "center" wire.

Using the table translations any region of interest within the wire strand can be brought into the probe volume for diffraction measurements. During our experiments we only measured the neutron scattering at the centers of the "Near", "Center" and "Far" wires at the sample midpoint, y=0, z=0. The probe volume placement was verified by doing intensity scans as a function of "*x*" position. As can be inferred from Fig. 4(b), maxima in integrated intensity are expected whenever the probe volume is completely contained within a wire; intensity minima are expected whenever the probe is centered between wires. We performed intensity scans, with a 1 mm step size, after each loading step (Fig. 5) to ensure that no shifting of the wire positions with load occurred. In this figure, the centers of the "Near", "Center" and "Far" wires are at $x=5$ mm, 0 mm, and −5 mm respectively. The minimum at x= −2.5 mm corresponds to the boundary between the "Near"

[5] Crosby G-450, or equivalent, wire rope clips were used.

[6] This enables the acquisition of diffraction data from the axial and transverse directions simultaneously [11].

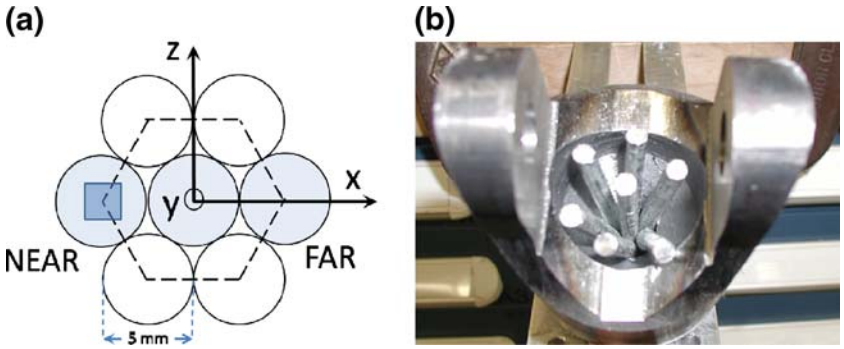

Fig. 2 **(a)** Scale drawing of the wire bundle cross-section; wire diameter is 5 mm (0.192”). The coordinate system used in the experiment is also shown. The dark square within the “Near” wire depicts the neutron beam cross-section. **(b)** Grip configuration for sample A. The outer wires are broomed out within the central cavity. The central wire was also bent to the side, and the wires were pulled back into the socket before the grip cavity was filled with epoxy

and “Center” wires. We do not observe a noticeable intensity drop between the “Center” and “Far” wires due to low scattering intensities. The vertical position of the bundle center (the z values in mm in the legend of Fig. 5) was monitored by an electronic dial gage (marked “D” in Fig. 3) at all times. During loading the wire bundle straightened, and the “z” value changed slightly, causing a shift of the center of the bundle cross-section with respect to the neutron beam. This shift was eliminated by moving the sample table up or down, using the z translation, to compensate for the displacement shown by the dial gage.

Once the sample position was verified at a given load, the spallation-neutron scattering patterns in both detector banks were recorded from the center of each wire. Typical data are shown in Fig. 6, where the abscissa values (atomic plane spacing) correspond to the time-of-flight of neutrons detected by the detector banks [11]. The peaks in this figure yield the atomic plane spacings, d_{hkl}, of particular sets of lattice planes, where h, k, l denote the Miller indices of the diffracting set. Elastic strains will cause these plane spacings to change; this is the basis of stress/strain measurements with x-ray or neutron diffraction techniques [11]. For relative strain changes, one can either use the variation of individual d_{hkl} with applied load, or combine all measured d_{hkl} to calculate a, the lattice parameter of the material. The latter process yields better statistics. We used Rietveld refinement [13, 14] with the Los Alamos GSAS program [15] to obtain the lattice parameters of the BCC ferrite phase of the ASTM A586 wire in the axial (loading) and transverse directions, a_y and a_x. The elastic strains

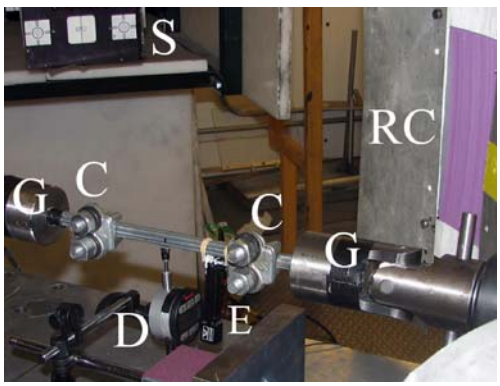

Fig. 3 Sample B mounted in the load tester of the SMARTS Diffractometer. The neutron beam from the incident slit (S) impinges on the sample directly above the tip of the dial indicator (D), at the black mark. The extensometer (E) is secured with rubber bands against a bottom wire. The cable clips, C, at each end, exert clamping forces on the entire wire cross-section, including the center wire. The center wire ends approximately 10 mm before entering the conical grips (G). The aperture of one of the radial collimators (RC) is also seen. There are beam-shields on both sides of the RC aperture to minimize stray radiation and background. In this figure the sample table has been lowered below the incident slit height to aid visualization

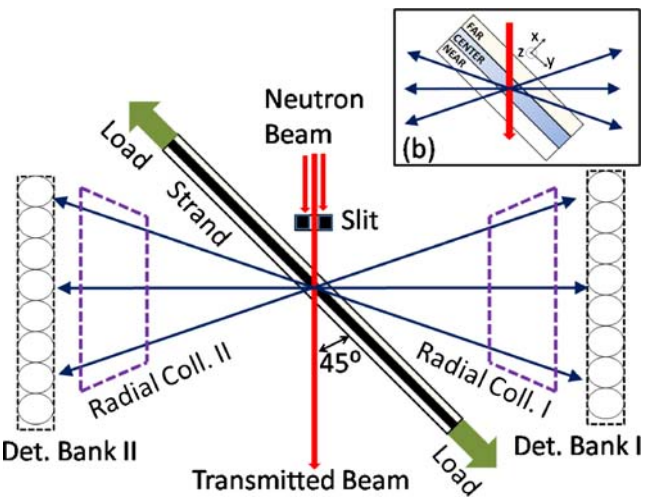

Fig. 4 Schematic of the SMARTS Diffractometer. The intersection of the incident beam and the acceptance fans of the radial collimators define the probe volume (inset). The entire load frame is mounted on a precision translator and can be moved to bring the center of each wire into coincidence with the probe volume. In this schematic, the longitudinal strains are measured by detector bank II

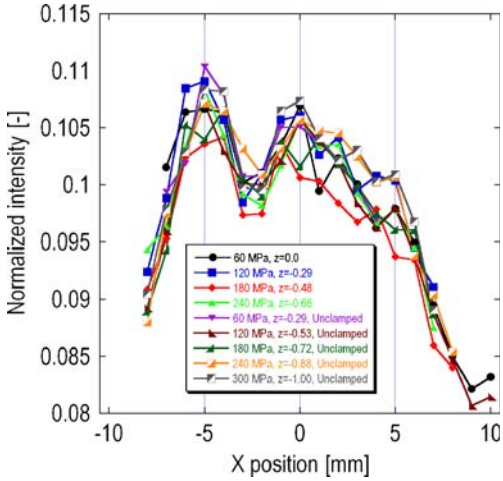

Fig. 5 Intensity vs. position scans of sample B taken before each loading cycle. The profile is stable over all loads. To obtain this data the sample was translated through the probe-volume (Figs. 2, 4) in steps of 1 mm. The maxima in the intensity position correspond to the center of the wires. The three vertical lines denote the measurement positions for "Near", "Center" and "Far" wires. Since the beam is 2 mm wide, zero intensity is achieved around 9 mm. We could not reach zero intensity in the negative x direction due to interference between the translator and the collimator mounts. The z values shown in the box are the positions of the wire bottom measured by the dial indicator (D in Fig. 3). The table was moved to compensate for these vertical position changes. Exact and identical placement of the neutron beam at each load is critical to ensure the integrity and comparability of strain data obtained at various loads

along the axial and transverse directions, $\varepsilon_{yy}, \varepsilon_{xx}$ were then computed from:

$$\varepsilon_{ii} = (a_i - a_0)/a_0,$$

where i=x or y, and a_0 is the unstressed lattice parameter. We used the lattice parameter at the initial preload as a_0. As a result of this approximation, the strains calculated from the lattice parameters are the elastic strains induced by the applied load only; no information about the residual elastic strain state in the wires is obtained. This approach is justified since we are only trying to determine the partitioning of the applied load between the constituent wires of the test strands. To ensure that the residual strain state within the wires did not change, the maximum applied load during the neutron strain measurements was kept 100 MPa below the maximum applied load used in the pre-loading cycles. We also compared the diffraction profiles and lattice parameters of individual wires before and after the final loading cycles. No significant changes were observed.

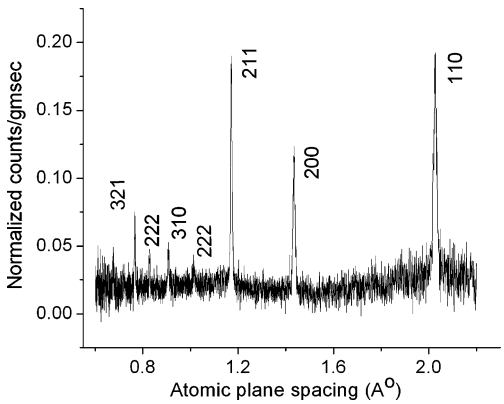

Fig. 6 A typical time-of-flight neutron scattering pattern. The individual peaks correspond to particular sets of atomic planes; the indices of the first seven sets are shown. The total profile is refined to obtain the lattice parameter of the material along a given sample direction

The error bars for the longitudinal strains, obtained from the GSAS program, were about 20 microstrain for all three wires. At the same time, the corresponding error bars (estimated standard deviation, ESD, from the Rietveld fitting) for the "Far", "Center", and "Near" wires in the transverse bank were about 175, 50 and 20 microstrain respectively. The large errors associated with the transverse strain values from the "Far" wire are due to the significant attenuation of the neutron beam. The total neutron path in this case is approximately 45 mm of steel. In addition, the Poisson strains in the transverse directions are only a third of the longitudinal strains. Thus, for the counting times we employed, the transverse strain data is noisier. Consequently, we only used the longitudinal strain values to study the relative load partitioning.

Results and Discussion

Sample A

Sample A, with all seven wires captured in the conical grips, was tested first. Variation of the longitudinal neutron strains in the "Near", "Center", and "Far" wires, and the transverse strains in the "Near" and "Center" wires are shown in Fig. 7. The transverse strains measured from the "Far" wire were anomalous due to bad counting statistics and could not be analyzed. Qualitatively, we observed the expected behavior: expansion of the lattice in the longitudinal direction and contraction in the transverse direction. There is, however, significant variability between the strains within the individual wires: the slopes of best-fit lines to the longitudinal data are 7.1(0.2), 2.7(0.2), and 3.7 (0.2), for the "Near", "Center", and "Far" wires respectively.[7] Thus, the central wire carries approximately 0.4× of the load carried by the "Near" wire, and 0.7× of the load carried by the "Far" wire. This variability appears to stem from the uneven loads exerted by the conical grips. This

[7] The lines shown in Figs. 7, 8, 9 and 10 simply connect the points to guide the eye. We used linear least-squares regression fit to obtain the slopes used in the analysis.

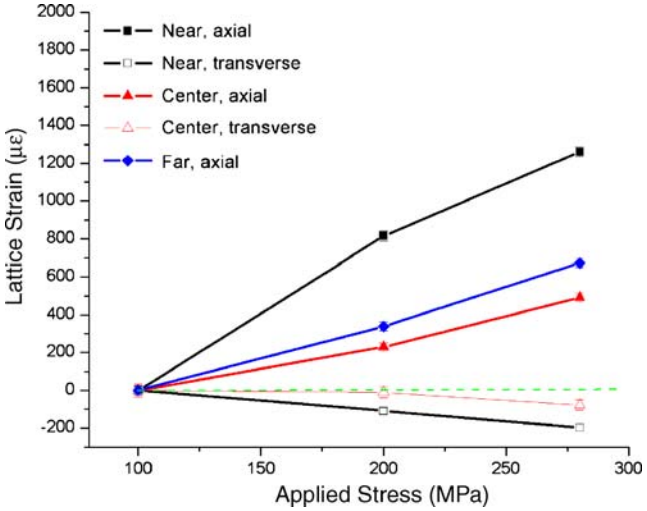

Fig. 7 Variation of elastic lattice strain vs. applied load in sample "A". The axial lattice strains from the three central wires defined in Fig. 2(a) all increased linearly with applied load. The transverse strains decreased due to Poisson coupling. The lines shown simply connect the points to guide the eye

conclusion is supported by the neutron-strain vs. load response of sample B discussed below.

Sample B

i- "Tightly Clamped" condition

In this case, the clamps at the ends of sample B ("C" in Fig. 3) were tightened to 135 N-m before the tensile load was applied. Variation of the transverse and longitudinal neutron strains in the "Far", "Center", and "Near" wires are shown in Fig. 8. The strain partitioning in this case is more uniform; the slopes of best-fit lines to the axial strain data are 3.4 (0.2), 4.7 (0.2), and 5 (0.2), for the "Near", "Center", and "Far" wires. The "Near" wire carries approximately 0.7× of the load carried by the "Far" wire. The central wire, which does not go into the grips, carries a load comparable to the "Far" wire. This load is almost 1.4 times the load carried by the "Near" wire, which is captured in the grips. This may be due to the significant radial force provided by the heavily torqued clamps. The wire bundle was bent near these clamps, with resultant mechanical interference between the wires in addition to shear loading at surfaces.

ii- "Loosely-Clamped" condition

In this case, the clamp bolts at the ends of sample B were loosened, tightened to 14 N-m, loosened again and then set finger-tight. We then cycled the applied stress between 50 MPa and 350 MPa three times to minimize interference effects between neighboring wires. We then acquired neutron lattice strain data at 60, 120, 180, 240 and 300 MPa nominal stress values. The axial and transverse neutron strains as a function of applied load in the three wires are shown in Fig. 9. Comparison of Figs. 8 and 9 shows that loosening the clamp has not changed the load distribution significantly: the slopes of best-fit lines to the axial strain data are 3.1 (0.2), 4.0 (0.1), and 4.8 (0.1), for the "Near", "Center", and "Far" wires. The central wire has shed some load, but it is still carrying 1.3 times more load than the "Near" wire. The mechanism of load transfer to the central wire in this case is still ambiguous: while the clamping load is much smaller, the radial/mechanical constraint imposed by the clamps on the bundle might prevent the "bent" ends of the central wire to straighten

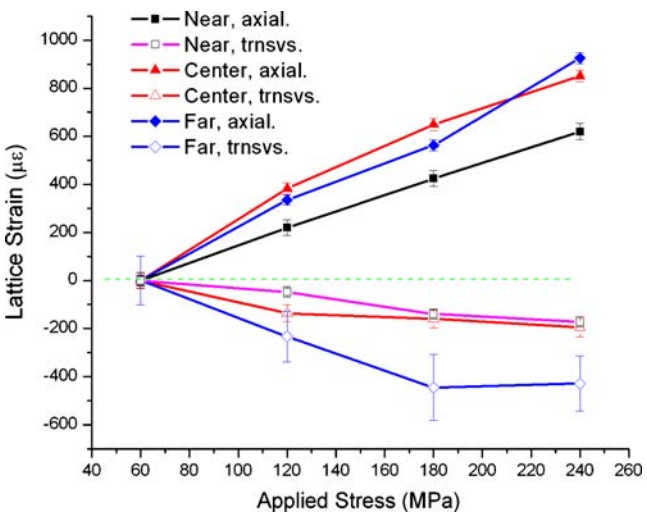

Fig. 8 Variation elastic of lattice strain vs. applied load in sample "B", loaded in the "clamped" condition. Even though the "Center" wire did not go into the grips, the clamps provided sufficient constraint for efficient load transfer to this wire

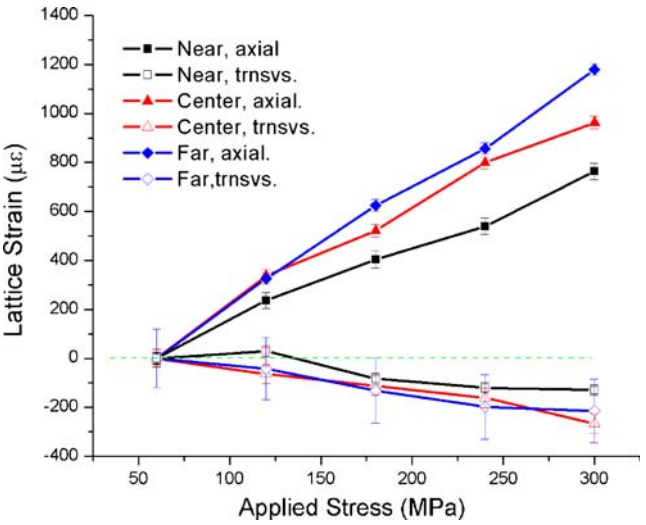

Fig. 9 Variation of elastic lattice strain vs. applied load in sample "B", loaded in the "loosely-clamped" condition. In terms of load sharing behavior, there was very little change from the "clamped" condition

and slip past its neighbors. Thus, both shear over the entire contact surface and mechanical interference mechanisms could contribute to the total load transfer. Our results show that, once the clamps were loosened, the Near and Far wires carried approximately the same load as before (within error) while the load carried by the Center wire dropped approximately 15%. This result would violate equilibrium if these were the only three wires carrying the total load. However, there are four more wires which are captured in the grips; it is possible that the load shed by the central wire was distributed over these four wires.

iii- "Unclamped" condition

To test how much of the strain transfer was due to the friction at the wire boundary, one clamp was completely removed, and the second clamp was moved closer to the center and finger tightened. Thus, relatively insignificant radial compressive forces are applied around a single point. Figure 10 shows the variation of transverse and longitudinal neutron strains with applied load for this condition. The slopes of best-fit lines to the axial strain data are 5.2 (0.2), 1.9 (0.2), and 4.5 (0.2), for the "Near", "Center", and "Far" wires. The center wire has shed 50% of the load it carried in the lightly-clamped configuration, while the load carried by the "Near" wire has gone up by 1.7×. It is surprising that the center wire still carries approximately 0.4× of the load carried by the continuous wires. The load transfer in this case should be mainly due to the shear at the wire boundary. However, there could still be some mechanical

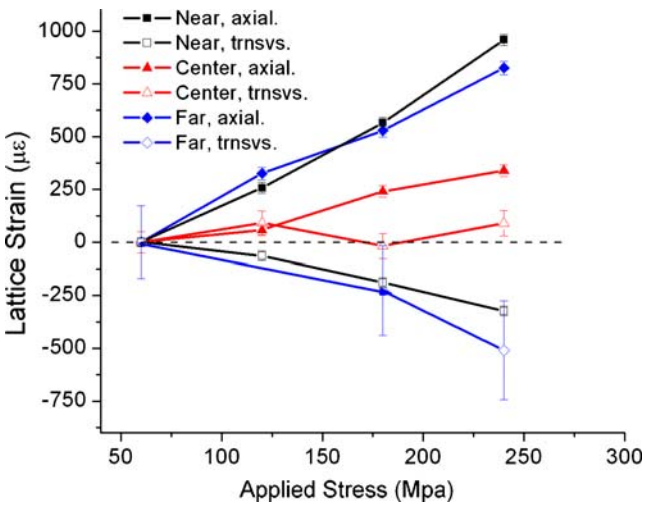

Fig. 10 Variation of lattice strain vs. applied load in sample "B", loaded in the "unclamped" condition. In this case, one of the clamps (C in Fig. 3) has been removed, and the other moved within two inches of the center (black dot in Fig. 3). The "Center" wire, which is not captured in the grips, has shed 50% of the load it carried in the lightly-clamped configuration, while the load carried by the "Near" wire has gone up by 1.7×

constraint by the radial forces exerted on the central wire by the outside wires. Using the maximum strain measured at sample midpoint, and assuming a hyperbolic cosine function dependency on strain transfer with length [16], the length of the wire bundle (approximately 310 mm) should be comparable to the development (recovery) length over which the elastic strain in a broken wire builds up to the value carried by an unbroken one. The build-up of elastic strain with distance from a broken end, and the distance over which clamping effects decay will be measured in future experiments.

Summary and Conclusions

In this study we used neutron diffraction to measure the longitudinal elastic strains induced within individual wires of two seven-wire cable strands in response to loads applied by a tensile tester. Differences in these measured strains yielded directly the partitioning of the applied load between these wires.

Our first sample was a standard seven-wire cable strand with conical grips. The wires were broomed-out within the grips and fixed with socket epoxy. We observed that this type of grip construction was not able to provide uniform load partitioning between the wires; the loads carried by adjacent wires could be different by 2.5× at the midpoint of the strand. A better grip configuration, with much tighter load distribution within the wires, is required for more quantitative studies. This work is underway, and will be reported later.

In our second sample, the center wire terminated 10 mm *before* entering the socket assemblies at each end. Thus, there could be no direct load transfer to the central wire from the grips; load could only be transferred to this wire from the surrounding six wires through friction and/or mechanical constraint at the contact surfaces. Our data show that friction between wires is an important mode of strain transfer: the longitudinal elastic strain at 150 mm distance from the broken ends of the central wire of the seven-wire strand was approximately a quarter of the elastic strains carried by unbroken outer wires. Clamping the strand loosely at both ends using wire-rope clips significantly increased the strain transfer. Such clamping kept the bundle together and, possibly, increased the mechanical interference and total contact area between the central wire and its neighbors. In the fully clamped condition the central wire, which had no direct connection to the grips, carried more load than a neighboring wire which was captured in both grips. Thus, clamping can be used to enhance strain transfer to broken inner wires in wire cable assemblies.

In summary neutron strain transfer measurements in test strands of parallel-wire suspension-bridge cables are feasible and can yield valuable data. We were successful in

measuring elastic strain partitioning across the cross-sections of two seven-wire strands with neuron diffraction. To our knowledge, these are the first measurements of this kind. Similar studies can yield insight into the strain partitioning in strands prepared with different conditions. A systematic study of load sharing in wire rope and bridge cable assemblies will yield valuable data for testing and improving analytical calculations [3, 17] and finite-element models [18, 19]. Such results would also contribute to the evaluation of the load carrying capabilities of existing suspension-bridge cables, and to the design of new bridge cables. These studies are in progress and will be reported later.

Acknowledgements We would like to thank Dr. Donald W. Brown (MST-8, Los Alamos National Laboratory) for helping plan the experiment. The samples were manufactured by Mr. Johny Manchery, Senior Laboratory Technician, of the Carleton Laboratory of Columbia University. Mr. Thomas A. Sisneros from Lujan Center modified the grips and assisted with the sample set-up. We thank Prof. Chris Marianetti of Columbia University for discussions and for welding the wires in Specimen B. This work has benefited from the use of the Lujan Neutron Scattering Center at LANSCE, which is funded by the Department of Energy's Office of Basic Energy Sciences. Los Alamos National Laboratory is operated by Los Alamos National Security LLC under DOE Contract DE-AC52-06NA25396.

References

1. Costello GA (1997) Theory of Wire Rope. 2 edn. Mechanical Engineering Series. Ling FG (ed). Springer Verlag, New York
2. Feyrer K (2007) Wire ropes: tension, endurance, reliability. Springer Verlag, Berlin
3. Fu G, Moses F, Khazem DA (2000) Strength of Parallel Wire cables for Suspension Bridges. in 8th ASCE Specialty Conference on Probabilistic Mechanics and Structural Reliability. University of Notre Dame, Notre Dame, Indiana: American Society of Civil Engineers
4. Utting WS, Jones N (1985) Tensile testing of a wire rope strand. J Strain Anal Eng Des 20(3):151–164
5. Utting WS, Jones N (1987) The response of wire rope strands to axial tensile loads .1. Experimental results and theoretical predictions. Int J Mech Sci 29(9):605–619
6. Utting WS, Jones N (1987) The response of wire rope strands to axial tensile loads .2. Comparison of experimental results and theoretical predictions. Int J Mech Sci 29(9):621–636
7. Raoof M, Kraincanic I (1998) Determination of wire recovery length in steel cables and its practical applications. Comput Struct 68(5):445–459
8. Cappa P (1988) An experimental-study of wire strains in an undamaged and damaged steel strand subjected to tensile load. Exp Mech 28(4):346–349
9. Wilson C, MacFarlane J (2000) Failure of wire rope sockets under impact loading. E D P Sciences
10. Bourke MAM, Dunand DC, Ustundag E (2002) SMARTS—a spectrometer for strain measurement in engineering materials. Springer-Verlag
11. Brown EN et al (2008) *In-situ* measurement of crystalline lattice strains in polytetrafluoroethylene. Exp Mech 48(1):119–131
12. Bourke MAM, Roberts JA, Davis D (1997) Macrostrain measurement using radial collimators at LANSCE. In: International Conference Neutrons in Research and Industry. SPIE, Crete, Greece
13. Rietveld HM (1967) Line profiles of neutron powder-diffraction peaks for structure refinement. Acta Crystallogr 22:151–2
14. Rietveld HM (1969) A profile refinement method for nuclear and magnetic structures. J Appl Crystallogr 2:65
15. Vondreele RB, Jorgensen JD, Windsor CG (1982) Rietveld refinement with spallation neutron powder diffraction data. J Appl Crystallogr 15:581–589
16. Murray CE, Noyan IC (2002) Finite-size effects in thin-film composites. Philosophical Magazine A-physics of condensed matter structure defects and mechanical properties. 82(16):3087–3117
17. Ghoreishi SR et al (2007) Analytical modeling of synthetic fiber ropes. Part II: a linear elastic model for 1+6 fibrous structures. Int J Solids Struct 44(9):2943–2960
18. Ghoreishi SR et al (2007) Validity and limitations of linear analytical models for steel wire strands under axial loading, using a 3D FE model. Int J Mech Sci 49(11):1251–1261
19. Jiang WG, Warby MK, Henshall JL (2008) Statically indeterminate contacts in axially loaded wire strand. Eur J Mech A-Solids 27(1):69–78
20. Brockenbrough LR, Merrit FS (2006) Structural steel designer's handbook. The McGraw-Hill Company, New York